RSC Advances

ROYAL SOCIETY OF CHEMISTRY

www.rsc.org/advances

Diketopyrrolopyrroles disubstituted with alkylated thiophenes: effect of the donor unit size and solubilizing substituents on their redox, photo- and electroluminescence properties

Gabriela Wiosna-Salyga[a]*, Monika Gora[b], Malgorzata Zagorska[c]**, Petr Toman[d], Beata Luszczynska[a], Jiri Pfleger[d], Ireneusz Glowacki[a], Jacek Ulanski[a], Jozef Mieczkowski[b] and Adam Pron[c]***

[a]*Department of Molecular Physics, Lodz University of Technology, Zeromskiego 116, 90-924 Lodz, Poland*
[b]*Faculty of Chemistry, Warsaw University, Pasteura 1, 02-093 Warsaw, Poland*
[c]*Faculty of Chemistry, Warsaw University of Technology, Noakowskiego 3, 00-664 Warsaw, Poland*
[d]*Institute of Macromolecular Chemistry AS CR, Heyrovsky Sq. 2, 162 06 Prague 6, Czech Republic*

* email: gabriela.wiosna-salyga@p.lodz.pl
** email: zagorska@ch.pw.edu.pl
*** email: apron@ch.pw.edu.pl

Abstract

Systematic studies of redox, spectroscopic and electroluminescent properties of donor-acceptor-donor (DAD) electroactive compounds consisting of diketopyrrolopyrrole central accepting unit symmetrically disubstituted with mono-, bi- or terthiophene (**T1**, **T2** and **T3** series) are presented. The potential of the diketopyrrolopyrrole unit reduction is influenced neither by the type of alkyl substituents at pyrrole nitrogen atoms, nor the position of alkyl substituents in thiophene rings of the D segment. Being in the range of -1.66 - -1.67 V vs Fc/Fc^+ in the compounds of **T1** series it is, however, raised by 100 - 120 mV for the **T3** series compounds. The oxidation potential of the studied compounds is even more strongly affected by D segment decreasing from 0.51 - 0.52 V in **T1** compounds to 0.25 - 0.26 V vs Fc/Fc^+ in **T3** ones. It is also dependent on the position of the alkyl solubilizing substituent in the thiophene ring being raised by *ca*. 40 mV by changing the alkyl substituent position from 5 to 3**.** The electrochemical data are in perfect agreement with the spectroscopic ones as judged from close similarity of the optically- and electrochemically-determined band gaps. The trends observed experimentally are reproduced in DFT calculations. The calculated values of ionization potentials and electron affinities are very close to the experimental ones. The highest photoluminescence quantum yield approaching 80%, was measured for **T1** compounds, whereas for **T3** ones its value dropped below 20%. Time resolved photoluminescence studies consistently showed in turn shorter emission lifetimes and larger non-radiative rate constants for compounds of lower photoluminescence quantum yields. Guest/host-type single layer light emitting diodes were

fabricated from the most luminescent compounds (**T1** series), molecularly dispersed (1 wt%) in a matrix consisting of 70 wt% of poly(*N*-vinylcarbazole) and 30 wt% of 2-tert-butylphenyl-5-biphenyl-1,3,4-oxadiazole. Appropriate alignment of the matrix components energy levels and those of the **T1** compounds resulted in effective electroluminescence of the guest molecules. The fabricated diodes showed luminance exceeding 2600 cd/m^2 with the luminous efficiency of 0.7 cd/A.

Introduction

Dithienyl diketopyrrolopyrrole (DT-DPP) being itself an interesting semiconductor, is frequently used as a building block for preparing semiconducting compounds of donor – acceptor (DA) type showing interesting electronic and opto-electronic properties (see for example [1-6]).

The use of DT DPP in the preparation of a large variety of low and high molecular weight DA-type organic semiconductors was made possible through recent development in the C-C coupling strategies, involving Suzuki[7,8], Stille reagents[9,10], direct arylation[11,12] and in the case of polymers Yamamoto coupling.[13]

Diketopyrrolopyrrole-based compounds can be used as components of the active layers in field effect transistors.[2] In this respect their capability of conducting holes or electrons in the FET configuration is determined by a delicate balance of electron donating/accepting properties of the DT DPP and the π-conjugated units attached to it. Weak donors induce ambipolarity[13], whereas, for stronger donors p-type behavior is observed.[14]

Since DA semiconductors usually show a smaller band gap due to rehybridization of bonds in the DA unit, they are also suitable for the fabrication of organic solar cells where they are used as components of the active layer.[6,15]

DAD compounds consisting of diketopyrrolopyrrole disubstituted with either thiophene or oligothiophene deserve a special interest since they exhibit very interesting spectroscopic, electrochemical and structural properties (including capability of self-assembling).[8] Moreover, they also find applications in organic electronics. DT DPP itself can be used in the fabrication of organic FETs showing however field effect only in the p-channel configuration.[16] The same applies to compounds with longer thiophene segments such as terthiophene disubstituted DPP.[17] The discussed group of compounds also found their application as components of bulk heterojunction photovoltaic cells, exhibiting appropriate alignment of their HOMO and LUMO levels with respect to [70]PCBM. This applies for example to diketopyrrolopyrroles symmetrically disubstituted with alkylbithiophenes.[18]

In this paper we present a systematic study of the effect of the thiophene donor segment length and the position of the solubilizing alkyl substituents on redox and spectroscopic properties of thiophene (oligothiophene) – diketopyrrolopyrrole DAD semiconductors. The obtained experimental results are confronted with the DFT calculations which help to rationalize the observed trends. Special emphasis is to put on electroluminescence of these compounds and their use as dispersed luminophores in light emitting diodes (LEDs) of guest/host single layer type. To the best of our knowledge no reports have appeared to date describing the application of thiophene (oligothiophene) – diketopyrrolopyrrole DAD semiconductors in this type of devices.

Experimental

Synthesis

The detailed synthetic pathways leading to the studied compounds, together with references to the used preparation procedures can be found in the ESI† of this paper.

Electrochemical measurements

Cyclic voltammograms and differential pulse voltammograms of the synthesized compounds were registered using an Autolab potentiostat (EcoChemie) in the electrolytic medium consisting of the studied compounds dissolved in 0.1 M dichloromethane solution of Bu_4NBF_4. The measurements were performed in an inert atmosphere, using a platinum disk working electrode of the surface area of 3 mm^2, a platinum wire counter electrode and an Ag/0.1 M Ag^+ reference electrode consisting of an Ag wire immersed in 0.1 M solution of $AgNO_3$ in acetonitrile.

Photophysical studies

UV-Vis absorption spectra were recorded on a Carry 5000 (Varian) spectrometer. Steady state as well as time-resolved photoluminescence measurements were done on FLS980 (Edinburgh Instruments) spectrometer. The fluorescence lifetime investigations were performed applying time-correlated single-photon counting technique using EPLED 340 diode as an excitation source. Thin layers of the studied compounds were deposited on a quartz substrate by spin coating from chlorobenzene solutions. Absolute quantum yields (Φ_{fl}) were measured in an integrating sphere, coated inside with BENFLEC®, provided by Edinburgh Instruments. The concentration of the studied samples was adjusted so that the optical density at the peak of absorption was less than 0.1. The Φ_{fl} values were determined according to the following equation:

$$\Phi_{fl} = \frac{N_{em}}{N_{abs}} = \frac{\int \frac{\lambda}{hc}[I^s_{em}(\lambda) - I^r_{em}(\lambda)]d\lambda}{\int \frac{\lambda}{hc}[I^r_{ex}(\lambda) - I^s_{ex}(\lambda)]d\lambda} \quad (1)$$

where N_{abs} is the number of photons absorbed and N_{em} is the number of photons emitted by the sample placed in the integrating sphere, λ is the wavelength, *h* is Planck's constant, *c* is the velocity of light. I_{ex}^{r} is an excitation profile collected with cuvette with solvent (reference) inside the sphere and I_{ex}^{s} is the same profile when the solvent is replaced by cuvette with the sample, I_{em}^{s} and I_{em}^{r} are the emission spectra of the sample and solvent used as reference. The spectra obtained in the integrating sphere were spectrally corrected using the correction file valid for the sphere.

Calculations

Geometries of the molecular conformations of the studied DPP derivatives were fully optimized using hybrid Hartree–Fock / Density Functional Theory method B3LYP[19,20] with 6-31G(d,p) basis set. This method usually provides reliable ground-state conformations and other basic properties of π–conjugated molecules including their ions.[21-23] All quantum chemical calculations were done by means of the Gaussian 09 program[24] with standard settings. To reduce energy oscillations and increase numerical accuracy during the molecular geometry optimization, two-electron integrals and their derivatives were calculated using the pruned (99,590) integration grid, having 99 radial shells and 590 angular points per shell. During the geometry optimization the calculated molecules were assumed to be isolated (in vacuum) and no temperature corrections were applied. Different starting geometries were used in order to find the lowest energy conformers. The obtained equilibrium structures were checked by normal mode analysis (no imaginary frequency was found).

Geometries of the lowest energy conformers found in vacuum were used as the initial coordinates for subsequent optimization of neutral molecules, cations, and anions in a solution of dichloromethane at the B3LYP/6-31++G(d,p) level in order to determine adiabatic ionization potentials and electron affinities. The equilibrium polarizable continuum model (PCM) was used for the description of the solvation effects.[25]

The vertical absorption spectra in chlorobenzene solution were computed by the time dependent version (TD-) of the DFT method,[26-28] employing two different DFT functionals CAM–B3LYP and PBE0 with 6-31++G(d,p) basis set and PCM/B3LYP/6-31++G(d,p) molecular geometries. The CAM–B3LYP functional is the range-separated Coulomb-attenuated hybrid exchange-correlation functional, the PBE0 one is the pure functional of Perdew, Burke and Ernzerhof,[29,30] as made into a hybrid by Adamo.[31] Both of them have been shown to properly predict excitation energies for similar organic compounds.[32,33] Solvent effects in the

absorption spectra calculations were involved by non-equilibrium linear response PCM. Vibrationally-resolved structure of the lowest absorption and emission bands were calculated using the Franck-Condon method.[34-36] It assumes geometry optimization and subsequent calculation of vibrational frequencies of both initial and final states. Because the excited state frequencies have to be calculated numerically, this technique is very computational time demanding. For this reason, calculations were restricted to the chlorobenzene solution of EtHex-DPP-T1 and to the B3LYP/6-31(d,p) level. In order to include the solvent effects, both initial and final states were optimized including PCM equilibrium solvation. To get proper position of the 0-0 transition, energy of the excited state was calculated with the state-specific equilibrium solvation using self-consistent PCM calculation. This method computes the energy in solution by making the solute's electrostatic potential self-consistent with the solvent reaction field (so called external iteration approach).[37,38] Program Gaussian[24] includes an efficient prescreening scheme to choose the vibrational transitions most relevant for the convergence of the vibronic spectra. One of its main features is that it relies on a categorization of the transitions with respect to the number of simultaneously excited modes in the final state, called classes, and the maximum number of integrals to compute for each of these classes.[34] In order to increase reliability of the calculated spectra, the number of considered classes was increased to 12 and the maximum number of calculated integrals in each class to 10^9. The resulting stick spectra were convoluted by Gaussian functions with the half-width at half-maximum equal to 400 cm^{-1}.

Organic light emitting diodes and electroluminescence measurements

Devices were fabricated using standard sandwich approach to investigate the synthesized compounds as emissive dopants in guest/host type active layers in OLEDs. The following geometry was chosen: glass/ITO/PEDOT:PSS/matrix:dopant blend/LiF/Al. As the host matrix poly(*N*-vinylcarbazole) (PVK) mixed with 2-tert-butylphenyl-5-biphenyl-1,3,4-oxadiazole (PBD), in a weight ratio 70:30, was used. PVK and PBD were obtained from Aldrich and used without further purification. PEDOT:PSS (Baytron P purchased from H. C. Starck) was spin-coated onto pre-cleaned and oxygen plasma-treated indium tin oxide (ITO) substrates and annealed at 200 °C for 10 min in air. Subsequently the chlorobenzene solutions of blend containing 1 wt% of the dopant (DPP-T1 derivatives) were filtered through a 0.2 μm PTFE filter and spin-coated on the PEDOT:PSS film. After drying (at 90 °C for 30 min in a glove box) the substrate was transferred into a vacuum chamber where LiF (about 1 nm) and Al (50 nm) cathode was thermally deposited. The emitting area of each OLED was determined by overlapping of the two electrodes (4.5 mm^2). The thicknesses of the active layers were about 80 nm, measured with a profilometer (Dektak XT, Brucker).

The current-voltage-characteristics of the fabricated devices were measured with a Keithley 2400 Source Measure Unit. The EL spectra were recorded using MicroHR spectrometer and CCD camera 3500 (Horriba Jobin Yvon). A Minolta CS-200 camera was used to obtain the luminance and CIE coordinates of the emitted light. Devices encapsulated in a dry-box and non-capsulated devices were measured in ambient conditions showing negligible effect of encapsulation on their performance.

Results and discussion

The studied compounds are depicted in Chart 1. They can be divided into three groups consisting of a diketopyrrolopyrrole unit symmetrically disubstituted with thiophene (**T1** series) bithiophene (**T2** series) and terthiophene (**T3** series).

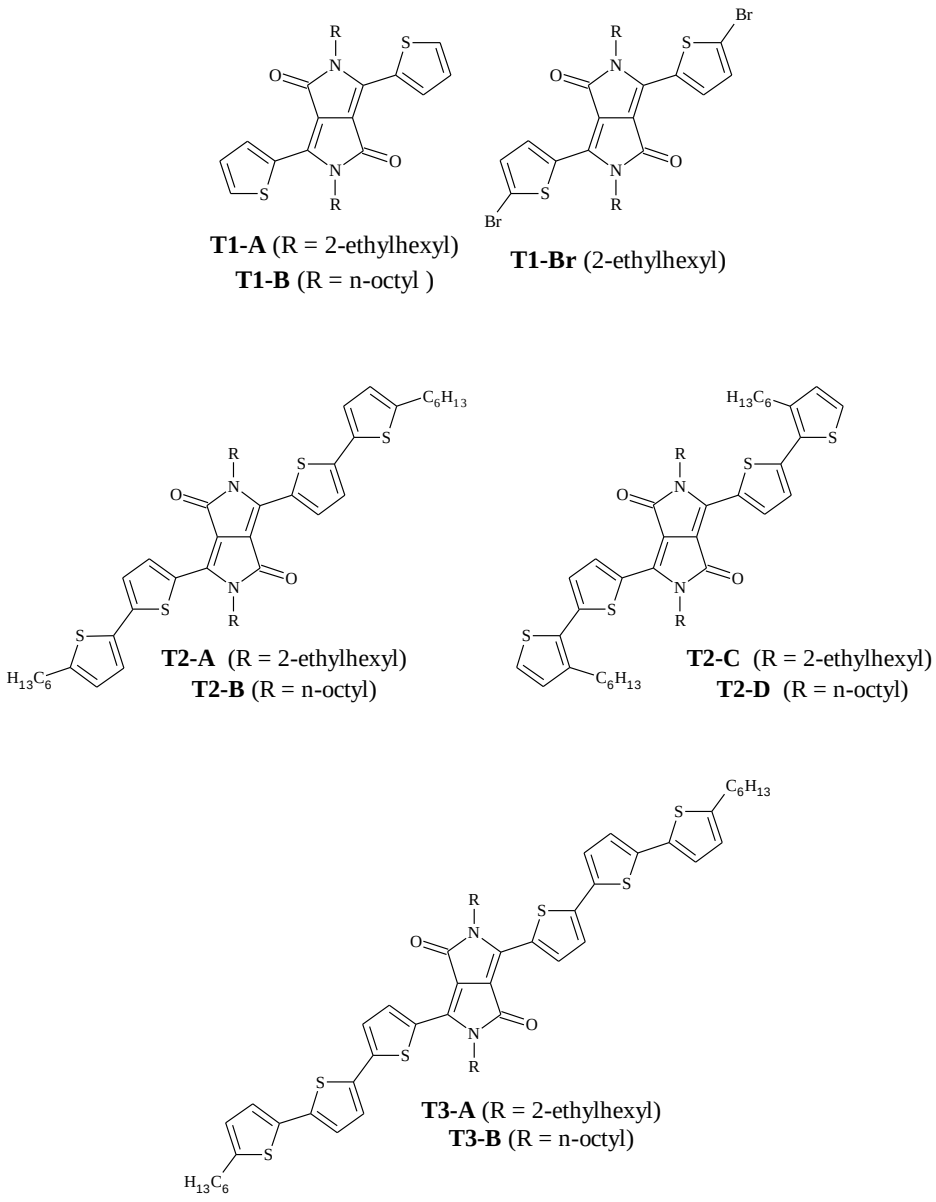

Chart 1 Structures of the studied compounds.

Electrochemical results vs DFT calculations

Representative cyclic voltammograms and the corresponding differential pulse voltammograms of the compounds studied are shown in Fig. 1. They consist of one redox couple at negative (*vs* Fc/Fc^{+}) potentials associated with the reduction of the diketopyrrolopyrrole central unit to a radical anion and its consecutive oxidation to the neutral state. At positive potentials two redox couples are observed attributable to the oxidation of the neutral molecule to a radical cation in the first step and to a dication in the second one. The oxidation process is accompanied by a rearrangement of bonds sequence from benzoid to quinoid (see Scheme 1).

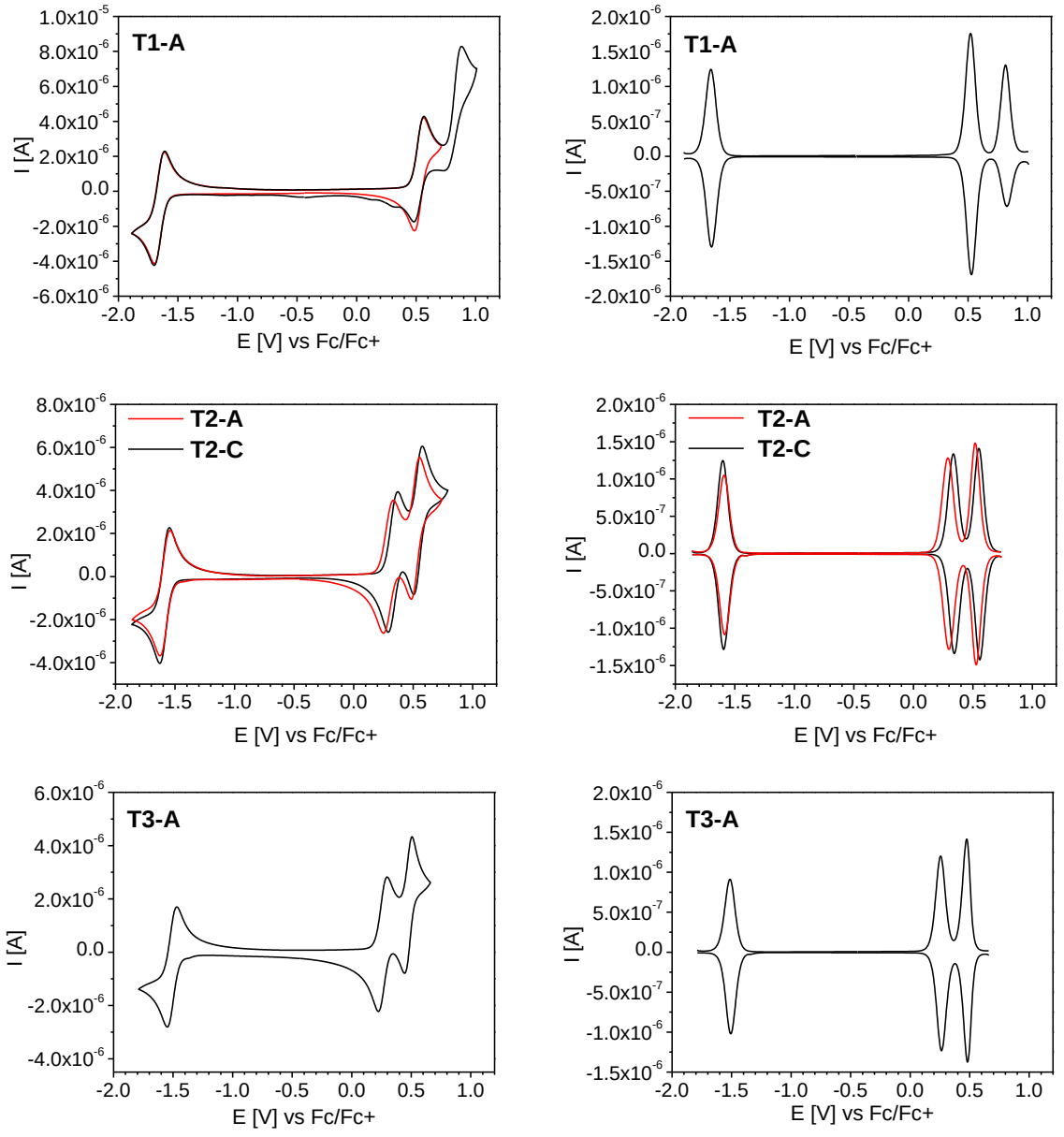

Fig. 1 a) Cyclic voltammograms (scan rate 50 mV/s) and b) differential pulse voltammograms (modulation time 50 ms, modulation amplitude 10 mV, step potential 5 mV) of **T1-A**, **T2-A**, **T2-C** and **T3-A**. Concentration of studied compounds: 10^{-3} M; electrolyte: 0.1 M Bu_4NBF_4/CH_2Cl_2; potentials are given *vs* ferrocene redox couple (Fc/Fc^{+}).

Scheme 1 Radical cation and dication forms of **T2** series compounds (hexyl substituents in the thiophene rings are not shown).

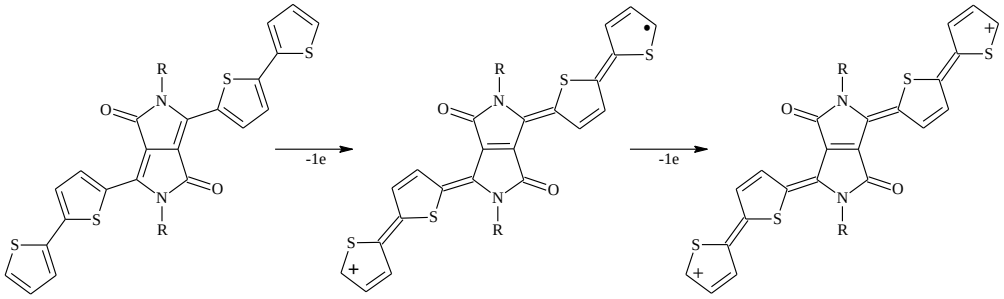

The spacing between the first and the second oxidation peak in the cyclic voltammogram is strongly affected by the length of D segment in the molecule. In **T1** series it exceeds 300 mV in **T2** series it is in the range of 220 – 230 mV, in **T3** one it drops to 200 mV. This trend can be unambiguously explained by the mechanism of the electrochemical oxidation. Removal of one electron in the first oxidation step creates a positive charge density in one of the two D segments. Abstraction of a second electron from the opposite D segment is affected by two factors: i) Coulombic repulsion between the introduced charges of the same sign and ii) the capability of delocalizing the positive charge imposed on the molecule during the first oxidation process. An increase of the D segment length lowers the Coulombic repulsion and facilitates charge delocalization through extension of the conjugation pathway.

Redox potentials of all compounds studied are listed in Table 1. The formal potential of the radical anion formation ($(E_{red1}+ E_{ox1})/2$) increases by *ca.* 100 - 140 mV when going from **T1** series to **T3** one. The effect of the type of alkyl substituents at pyrrole nitrogen atoms and the position of hexyl substituents in D segment thiophene rings is very small and does not significantly alter the reduction potential (compare data for **T2-A**, **T2-B, T2-C** and **T2-D** presented in Table 1). **T1-Br** is here an exception but it should be considered as an ADADA compound rather than a DAD one, which behaves differently.[39]

Table 1. Redox potentials given *vs* Fc/Fc^+, IP and EA obtained from electrochemical data and IP and EA calculated by DFT.

Sample	E_{red1} [V]	E_{ox1} [V]	$(E_{red1}+E_{ox1})2$ [V]	E_{ox2} [V]	E_{red2} [V]	$(E_{ox2}+E_{red2})/2$ [V]	IP_{el}[a] [eV]	EA_{el}[b] [eV]	E_g, [eV]	IP_{DFT}[c] [eV]	EA_{DFT}[c] [eV]
T1-A	-1.69	-1.62	-1.66	0.56	0.49	0.53	5.33	-3.14	2.19	5.25	-3.06
T1-B	-1.72	-1.62	-1.67	0.55	0.47	0.51	5.31	-3.13	2.18	5.24	-3.02
T1-Br	-1.62	-1.47	-1.55	0.61	0.54	0.58	5.38	-3.25	2.13	-	-
T2-A	-1.62	-1.54	-1.58	0.32	0.25	0.29	5.09	-3.22	1.87	4.92	-3.12
T2-B	-1.61	-1.53	-1.57	0.35	0.26	0.31	5.11	-3.23	1.88	4.91	-3.13
T2-C	-1.62	-1.55	-1.59	0.36	0.29	0.33	5.13	-3.21	1.92	5.02	-3.09
T2-D	-1.66	-1.56	-1.61	0.37	0.29	0.33	5.13	-3.20	1.93	5.00	-3.07
T3-A	-1.56	-1.47	-1.52	0.29	0.22	0.26	5.06	-3.28	1.78	4.85	-3.21
T3-B	-1.65	-1.49	-1.57	0.27	0.22	0.25	5.05	-3.24	1.81	4.84	-3.22

[a] calculated according to the formula $IP = |e|((E_{ox2}+E_{red2})/2 + 4.8)$ [eV]
[b] calculated according to the formula $EA = -|e|((E_{red1}+E_{ox1})/2+ 4.8)$ [eV]
[c] calculated for dichloromethane solutions

To the contrary, the potential of the first oxidation process ($(E_{ox2}+ E_{red2})/2$) is affected to a significantly larger extent by the length of D segment and the position of the hexyl substituent in it. It is essentially independent of the type of N-substituent (octyl *vs* 2-ethylhexyl, see **T2-C** and **T2-D** in Table 1). Extension of D segment from thiophene to terthiophene lowers the first oxidation potential by more than 250 mV. The position of the alkyl substituent in D also has a pronounced effect on the first oxidation process potential. Derivatives with the hexyl group in position 3 of the thiophene ring are more difficult to oxidize than those with the same substituent in position 5 (compare **T2-A** and **T2-C** in Table 1). This can be explained on the basis of optimized molecule geometry obtained from quantum chemical calculations which are presented in Fig. 2 for compounds with 2-ethylhexyl substituents at the nitrogen atoms. Optimized coordinates of all molecules can be found in ESI† of this paper (see Table S1 and S2).

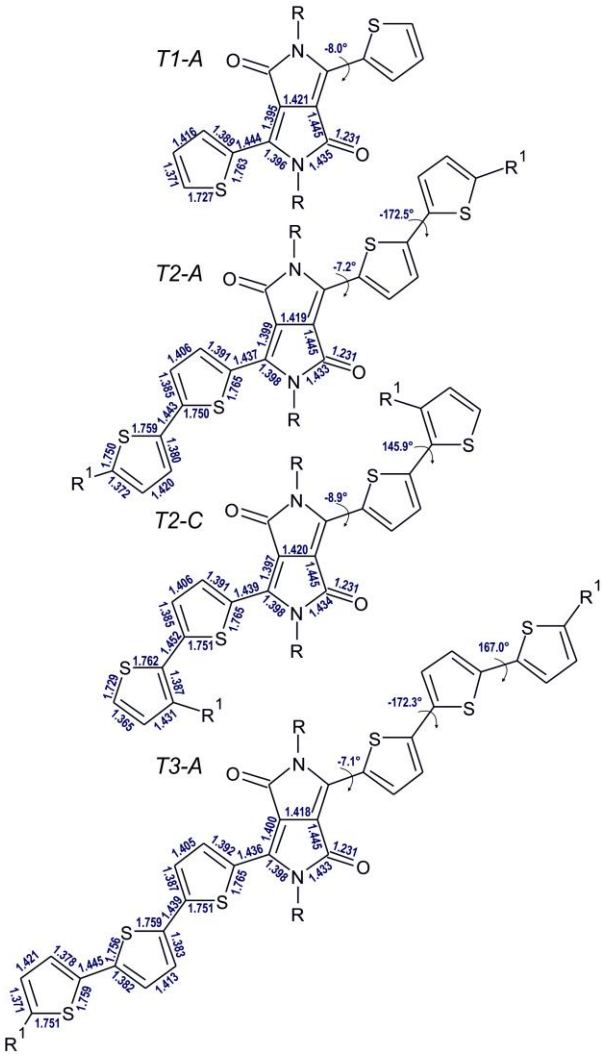

Fig. 2. Schematic structures of **T1-A**, **T2-A**, **T2-C** and **T3-A**; their optimal bond lengths (in Å) and dihedral angles (S-C-C-S and N-C-C-S) between the aromatic rings (in degrees) calculated using the B3LYP method with 6-31G (d,p) basis set in vacuum. Values for bonds and angles in symmetrical positions are not repeated.

Few generalizations can be made concerning the optimized geometry: the dihedral angle N–C–C–S between the diketopyrrolopyrrole core and the adjacent thiophene ring is close to 0º for linear alkyl N-substituents, for branched ones this torsion increases by ca. 10º. However, for molecules with the same N-substituent, the geometry is strongly influenced by the position of the alkyl substituent in the thiophene ring. The dihedral angle between the two adjacent thiophene rings are 145.9º and -172.5º for **T2-C** and **T2-A**, respectively. The obtained results of the geometry optimization are in line with those reported in the literature for similar derivatives (albeit, with different alkyl groups).[40-42]

This higher dihedral angle between the adjacent thiophene rings makes **T2-C** more difficult to oxidize as manifested by a higher potential of its first oxidation process and, by consequence, its higher ionization potential (IP). In Table 1 IP and electron affinities (EA) values derived from electrochemical measurements are compared with those calculated by DFT. Although the electrochemically determined IP and |EA| values are systematically higher by 0.10– 0.20 eV than the DFT calculated ones, the observed trends are essentially identical. This rather small systematic difference may originate from an overestimation of the extent of conjugation, leading to excessive delocalization of net charge in DFT methods, frequently encountered for π-conjugated ions. A very good correlation between the experimental and calculated values clearly indicates adequacy of both methods.

Spectroscopy in solution: experiment vs DFT calculations

In Fig. 3 the frontier orbitals of **T1-B** are shown as a representative example. For both HOMO and LUMO orbitals the electron density is spread over the whole conjugated part of the molecule. This delocalization also persists in derivatives with bi- and terthiophene substituents.

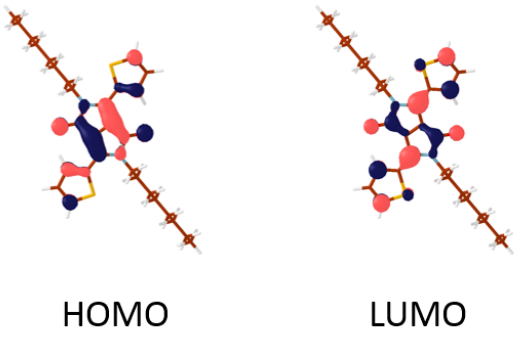

Fig. 3 Frontier orbitals of **T1-B** calculated by the B3LYP/6-31G(d,p) method in vacuum, contour 0.04.

The obtained frontier orbital shapes are in good agreement with those reported for similar derivatives, differing however by the type of alkyl substituents.[8,16,40-42,43]

In Fig. 4 representative UV-Vis spectra of the four studied derivatives, registered for chlorobenzene solutions are presented. The spectra of the remaining compounds can be found in ESI† of this paper.

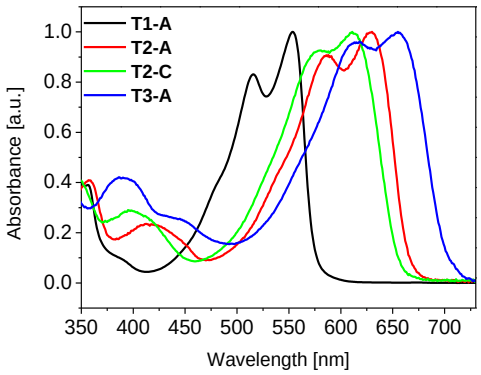

Fig. 4 Normalized UV-Vis absorption spectra registered for chlorobenzene solutions of **T1-A**, **T2-A**, **T2-C** and **T3-A**.

In each of this spectrum two bands can be distinguished. The first one of strongly vibronic character is located in the spectral range of 540 to 660 nm ($S_0 \rightarrow S_1$) and can be ascribed to the HOMO to LUMO (H→L) transition. As evidenced by CAM-B3LYP calculations the contribution of H→L transition to this band increases from *ca.* 91% for the **T3** series to over 98% for the **T1** one. PBE0 yields, in turn, almost the same H→L contribution for all compounds, in the range 98-99% (see Table 2). The second band can be attributed to the π–π* in the DPP central unit.

In Fig. 5 calculated spectra are compared for the same compounds whose experimental spectra are presented in Fig. 4, whereas in Table 2 the measured maxima of the absorption bands of all compounds studied are listed together with the calculated excitation energies for the dominant excitation, its oscillator strength and the contribution of the H→L transition to this excitation.

Theoretical spectra were calculated using two different methods, namely CAM-B3LYP and PBE0. Comparing the lowest excitation energies (see Table 2), it can be stated that both methods follow the experimentally found trends, but differences in excitation energies among samples are a bit overestimated, namely in PBE0 spectra. On the other hand, PBE0 results are closer to the experimental values, while CAM-B3LYP results overestimate the experiment by ca. 0.17 eV. The main difference between CAM-B3LYP and PBE0 methods is that CAM-B3LYP is a long-range corrected method, which should be more suitable for molecules with highly

delocalized excited states or charge transfer excitations. Improper long-range behavior of PBE0 together with different extents of conjugation in **T1** - **T3** derivatives is probably the cause for more significant overestimation of the trends in the excitation energies calculated by this method. Nevertheless, overall agreement of the absolute values between PBE0 results and experiment is very good.

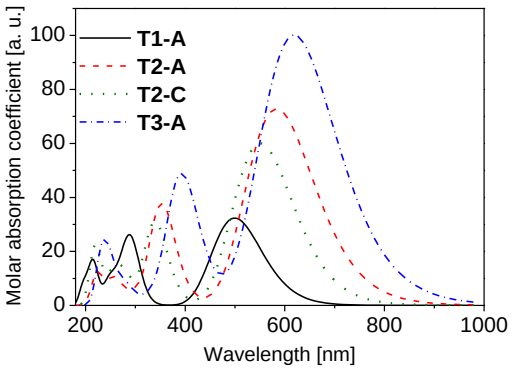

a)

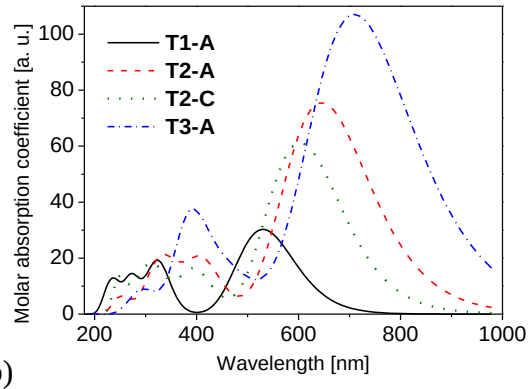

b)

Fig. 5 UV-Vis solution (chlorobenzene) spectra of **T1-A**, **T2-A**, **T2-C** and **T3-A**, calculated using a) TD CAM-B3LYP/6-31++G(d,p) method and b) TD PBE0/6-31++G(d,p) method.

The most intensive (H→L) band bathochromically shifts with increasing number of thiophene rings in D segment by *ca.* 100 nm when going from **T1-A** to **T3-A**, which can be considered as a spectroscopic manifestation of the π-π conjugation extension. The calculated oscillator strength for derivatives with different length of D segments are in agreement with the maximal excitation coefficient increasing with the number of thiophene rings.[44] The observed shift also depends on the position of the alkyl substituent. Moving it from position 5 of the terminal thiophene ring to position 3 induces an experimentally measured hypsochromic shift of this band by *ca* 20 nm (compare **T2-A** and **T2-C** in Table 2 and Fig. 4). This shift caused by steric effects is fully consistent with the calculated molecular geometry, indicating lower planarity of **T2-C**, and with the electrochemical data showing its more difficult oxidation (see

Fig. 2 and Table 1). Finally, in bromine capped **T1-Br** this band is bathochromically shifted by *ca.* 20 nm with respect to the corresponding band in **T1-A**, again manifesting the ADADA nature of this derivative.

A very good correlation is found between the calculated energy of the first excitation and the experimental position of the *0-0* transition band as shown in Fig. 6. Equally good correlation was established for electrochemical and optical band gaps (see Figure 7) unequivocally indicating high consistency of the electrochemical, spectroscopic and calculation results.

Table 2. Experimentally determined absorption bands (λ_{max}) and theoretical excitation energies, oscillator strengths as well as HOMO to LUMO contributions calculated using PCM/TD CAM-B3LYP/6-31++G(d,p) and PCM/TD PBE0/6-31++G(d,p) methods in chlorobenzene.

	Experiment		**TD CAM-B3LYP/6-31++G(d,p)**			**TD PBE0/6-31++G(d,p)**		
Sample	**Absorption band [nm]**		**Excitation energy [eV]/[nm]**	**Oscillator strength**	**HOMO to LUMO contribution [%]**	**Excitation energy [eV]/[nm]**	**Oscillator strength**	**HOMO to LUMO contribution [%]**
	Main band	**π-π***						
T1-A	552 (0-0) 515 (0-1) 470 (0-2)	354 343	2.48/500	0.70	97.97	2.34/530	0.66	99.03
T1-B	550 (0-0) 512 (0-1) 470 (0-2)	355 340	2.45/506	0.71	98.02	2.31/536	0.67	99.08
T2-A	627 (0-0) 586 (0-1)	412 355	2.12/584	1.58	94.83	1.92/645	1.64	98.89
T2-B	630 (0-0) 586(0-1)	413 356	2.09/592	1.61	94.92	1.90/653	1.68	98.91
T2-C	609 (0-0) 580 (0-1)	407 345	2.25/551	1.30	95.8	2.06/603	1.33	98.85
T2-D	610 (0-0) 579 (0-1)	405 344	2.22/559	1.35	95.89	2.03/611	1.38	98.89
T3-A	655 (0-0) 618 (0-1)	450 398	2.00/619	2.17	90.91	1.75/710	2.32	98.18
T3-B	655 (0-0) 615 (0-1)	440 392	1.98/626	2.21	91.24	1.73/716	2.38	98.21

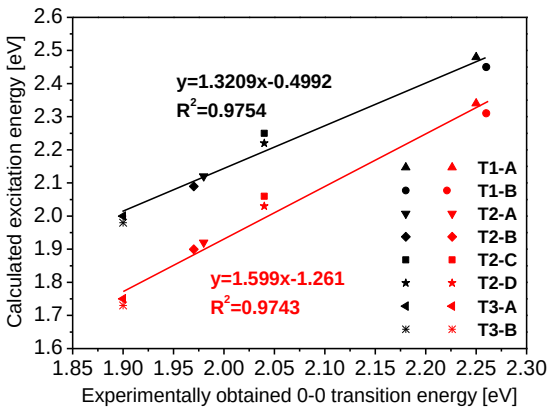

Fig. 6 Calculated excitation energy using PCM/TD CAM-B3LYP/6-31++G(d,p) (black) and PCM/TD PBE0/6-31++G(d,p) (red) method *vs* energy of the *0-0* transition obtained from absorption spectra.

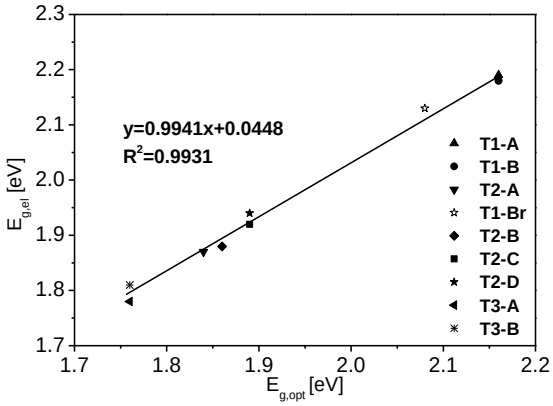

Fig. 7 Electrochemical *vs* optical band gap.

Representative emission spectra of the studied luminophores are shown in Fig. 8, whereas the spectra of other studied compounds are collected in the ESI†, Fig. S2. In the case of **T1** compounds a mirror image is obtained for the absorption and emission spectra (see Fig. 8) which suggests a similar geometry in the ground and excited states.

Relatively small conformational changes connected with the excited state relaxation were also confirmed by quantum chemical calculations using PCM/B3LYP/6-31(d,p) method. Subsequently calculated vibrationally-resolved structure of the lowest absorption and emission bands of the **T1-A** derivative is shown in Fig. 9. The calculated vibronic transitions are in a very good agreement with the experimental values – see Table 3. It should be pointed out, that even the use of a rather small basis set leads to a good agreement of the theoretically calculated vibronic spectra with the experimental ones. Better agreement is found in this case, than in purely electronic spectra shown in Fig. 5 and Table 2. This shows the importance of the vibrational structure considerations in the interpretation of the spectroscopic data.

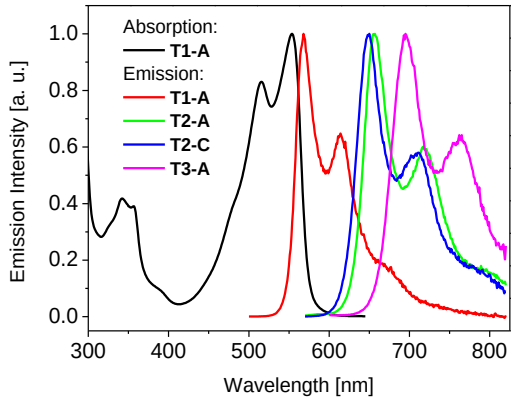

Fig. 8 UV-Vis absorption spectrum of **T1-A** and normalized emission spectra of **T1-A** (λ_{exc} = 340 nm), **T2-A** (λ_{exc} = 345 nm), **T2-C** (λ_{exc} = 360 nm) and **T3-A** (λ_{exc} = 390 nm) registered for chlorobenzene solutions.

Table 3. Comparison of experimental and theoretical (PCM/B3LYP/6-31(d,p)) vibronic transitions of the **T1-A** derivative in chlorobenzene solution.

Transition	Experimental wavelength [nm]	Theoretical wavelength [nm]
Absorption		
0–0	552	545
0–1	515	509
0–2	470	shoulder at 470
Emission		
0–0	569	556
0–1	614	599
0–2	670	shoulder at 667

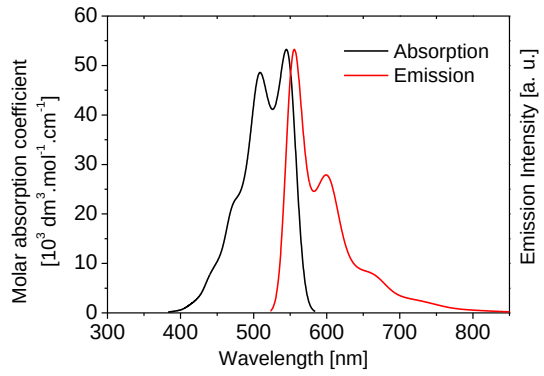

Fig. 9 Vibronic spectra of **T1-A** in chlorobenzene solution calculated using the Franck-Condon method at the PCM/B3LYP/6-31(d,p) level.

With increasing number of thiophene rings in D segment, the emission bands are being bathochromically shifted, the Stokes shift increases and the absorption and emission spectra partially loose their mirror symmetry. Although the vibronic structure of the absorption bands

becomes less pronounced in the case of compounds **T2** and **T3,** it is still preserved in their emission spectra. It indicates that the excited state geometry is more rigid than that of the ground state. It may be related to the excited state benzoid-quinoid canonical electronic structure transformation observed for oligothiophene solutions.[45]

Principal photophysical parameters obtained for all studied derivatives are collected in Table 4. A profound effect of the length of the donor segment on the photoluminescence quantum yield (Φ_{fl}) and its lifetime is observed. Monothiophene disubstituted derivatives exhibit Φ_{fl} values exceeding 75 %, reaching even 89 % for **T1-Br**. For compounds with bithiophene D segments Φ_{fl} decreases to *ca.* 40 % – 60 %, whereas in those with terthiophene D segments Φ_{fl} further drops below 20 %. This trend is typical for oligothiophene substituted DPP derivatives.[8,39,44] It may arise from several factors. In general small rigid molecules of localized conjugation, as for example diketopyrrolopyrrole fused central A unit, favor high emission efficiencies.[46] Attaching increasing number of thiophene rings to this central unit extends the conjugation but also lowers the rigidity of the molecule. Both factors contribute to an increase of the nonradiative energy dissipation and by consequence to a decrease of the photoluminescence quantum yield. Decreasing stiffness of the molecules with increasing length of the D segment is manifested by partial loss of the vibronic structure in the absorption spectra and an increase of the Stokes shift for **T2** and **T3** compounds as compared to **T1** ones. The extent of conjugation has, however, a more pronounced effect on the photoluminescence. This is manifested by a substantially higher quantum yield value measured for less conjugated **T2-C** as compared to **T2-A** – its more conjugated isomer. In addition, as the studied derivatives are donor-acceptor-donor (DAD) compounds, the role of charge transfer in the emission quenching mechanism should also be taken into consideration. Further studies are, however, needed to clarify the nature of the excited state depopulation process in the studied derivatives.

Finally, no or very little influence of the type of alkyl N-substituent on the photoluminescence quantum yield is observed (compare **T1-B** and **T1-A** or **T3-B** and **T3-A**). Correlated with decreasing quantum yield the emission lifetimes decrease upon extension of D segment from monothiophene to terthiophene. A consistent increase of the non-radiative constants values is also observed, which is especially pronounced for **T3** compounds (see Table 4).

Table 4. Photophysical parameters derived from stationary and time resolved spectroscopic measurements carried out for chlorobenzene solutions of studied compounds.

Sample	Emission band [nm]	Stokes shift [nm]	Photoluminescence quantum yield [%]	Emission lifetime [ns]	Radiative rate constant [10^8 s^{-1}]	Non-radiative rate constant [10^8 s^{-1}]
T1-A	569 614 670	17	75	5.8	1.3	0.4
T1-B	569 613 670	19	78	5.9	1.3	0.3
T1-Br	587 639 695	15	89	5.2	1.7	0.2
T2-A	657 720 790	30	45	2.3	2.0	2.4
T2-B	656 721 795	26	40	2.2	1.8	2.7
T2-C	649 709 790	40	58	2.7	2.1	1.6
T2-D	650 708 790	40	51	2.7	1.9	1.9
T3-A	695 760	40	14	0.8	1.8	10.8
T3-B	695 763	40	18	0.8	2.3	10.3

Spectroscopy in the solid state

The solid state absorption spectra of the studied derivatives were registered for thin films deposited on a quartz support by spin coating. In general three types of spectra are observed depending on the type of the derivatives, (see Fig. 10, where three representative examples are compared, other spectra can be found in ESI†): i) in the first type, the intensity sequence of vibronic bands is essentially the same as in the corresponding solution spectra *i.e.* the *0-0* band dominates, the *0-2* band is present only as a shoulder (spectra of **T1-B** and **T2-C**) ; ii) in the

second type, *0-0* and *0-1* are of comparable intensity, the *0-2* band still present as a shoulder (**T2-A**); iii) in the third type the *0-0* and *0-1* transitions are effectively quenched and the *0-2* band dominates the spectrum (**T1-A**, **T2-D** and **T3-A**).

Characteristic features of these three types of spectra can be interpreted in terms of the existence of J and H aggregates or a mixture of them. According to the exciton theory[47,48] the sign of the electronic coupling resulting from the molecular aggregation nature is responsible for the characteristic distortion of the absorption spectra. Thus, a bathochromic shift and narrowing of the absorption band in the solid state spectrum in comparison to the solution one is considered as a spectroscopic manifestation of the presence of J-aggregates (Fig. 10a**)**. On the contrary, a hypsochromic shift of the absorption maximum in the solid state spectrum is indicative of the H-aggregate formation (Fig. 10c).[44] Fig. 10b represents the case of co-existence of both types of aggregates. Spectra corresponding to both types of aggregates as well as to a mixture of them were reported for mono-, bi- and terthiophene substituted diketopyrrolopyrroles.[18,44] No clear correlation can be found between the length of D-segment as well as the position of alkyl substituent in D segment and the solid state spectral features. However, one can state that **T1** compounds with linear alkyl N-substituent (see Fig. S2 in ESI†) seem to favor the J-type aggregation. When some steric crowding is introduced by branched alkyl N-substituents, the H-type packing of the molecules in solid state is observed.

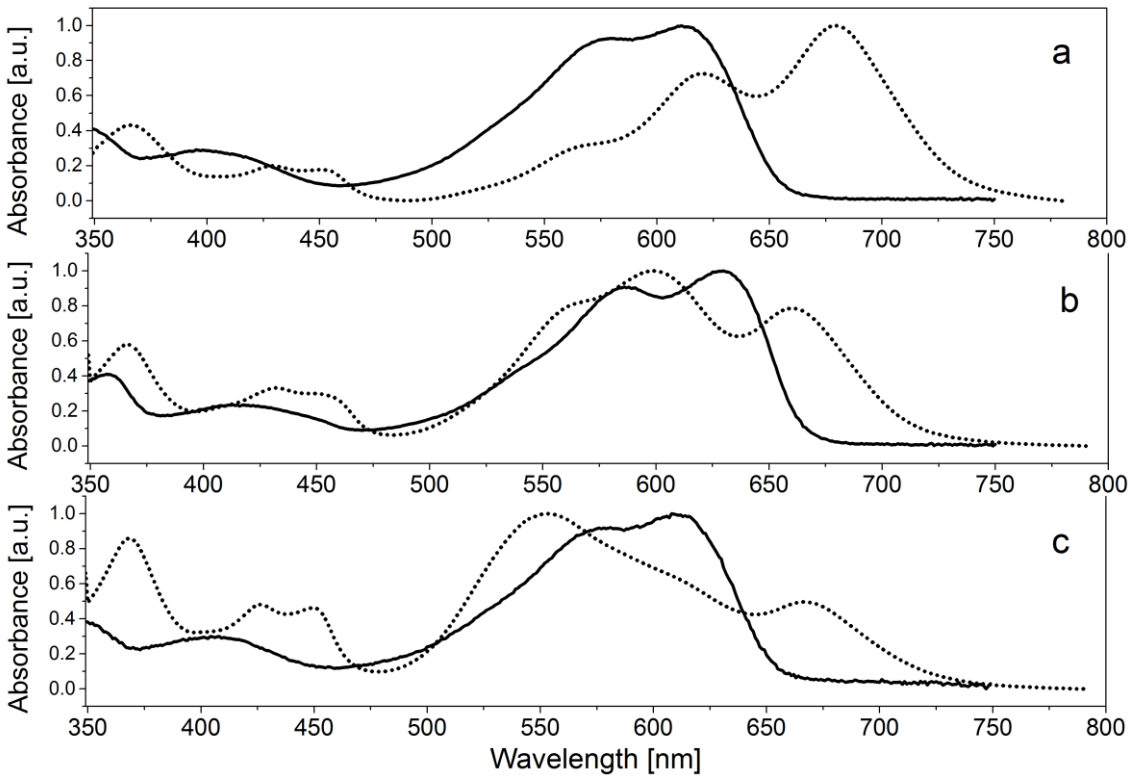

Fig. 10 Solution (solid line) and solid state (dotted line) absorption spectra of: a) **T2-C** (aggregates); b) **T2-A** (J+H aggregates) and c) **T2-D** (H-aggregates).

The emission spectra show a more complex nature since their shape is frequently affected by the thickness of the studied film and in addition depends on the excitation wavelength. Excitation at different energies, which match the energy of particular vibronic bands in the absorption spectrum, yields spectra in which the intensity sequence of the observed vibronic bands can vary. In the most frequent case the lower energetic vibronic bands dominate as demonstrated in the representative case of **T1-A** (see Fig. 11).

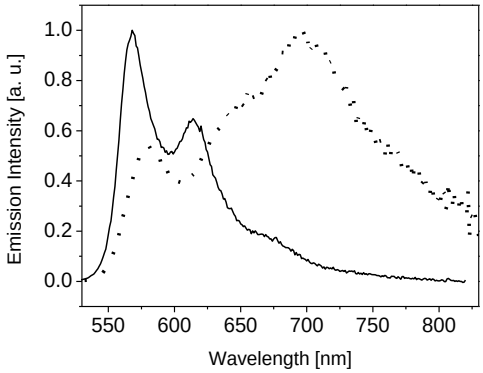

Fig. 11 Chlorobenzene solution (solid line) and solid state emission spectrum (dotted line) of **T1-A** (λ_{exc} = 520 nm).

In thin solid films the photoluminescence is effectively quenched due to aggregation of molecules and their strong interactions which provide the sites for non-radiative recombination (e.g. excimers) and reduce the probability of radiative emission. Moreover, the film forming properties of the studied derivatives are rather poor. For these reasons we were tempted to verify whether the excellent luminescent properties of the studied compounds (especially **T1** ones) can be exploited in light emitting diodes with a guest/host active layer where the aggregation induced luminescence quenching is avoided through molecular dispersion of the luminophore within an appropriate matrix.[49]

Electroluminescence and light emitting diodes

In Fig. 12 solution and solid state emission spectra of **T1-B** are compared with the spectrum of this compound molecularly dispersed in a matrix consisting of 70 wt% poly(N-vinylcarbazole) (PVK) and 30 wt% of 2-tert-butylphenyl-5-biphenyl-1,3,4-oxadiazole (PBD). This matrix is frequently used in guest/host LEDs as exhibiting appropriate alignment of the energy levels with a large number of luminophores and assuring ambipolar charge carriers transport.[50-52]

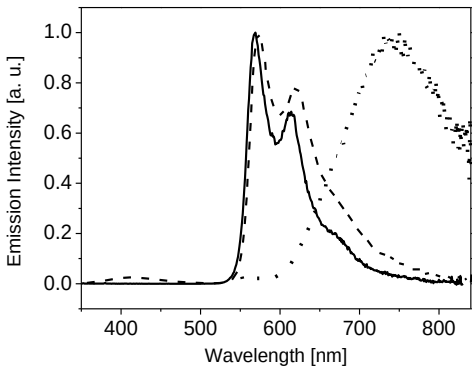

Fig. 12 Normalized emission spectra of **T1-B** registered for: chlorobenzene solution (solid line); thin solid film (dotted line); 0.7 wt% of **T1-B** dispersed in a solid PVK+PBD matrix (dashed line).

It can be noticed that the spectrum of **T1-B** in the PVK+PBD matrix is very similar to the solution one with two dominant vibrational bands bathochromically shifted by few nanometers. Note, that the emission in the blue region originating from the PVK+PDB matrix is almost nonexistent.

One of the possible mechanisms of the photo- and electroluminescence generation in the guest/host configuration is the Förster energy transfer from the host matrix to the guest molecules[53] which can occur when the emission spectrum of the host significantly overlaps with the guest's absorption spectrum. This condition is fulfilled for the **T1** and **T2** compounds (see Fig. 13 where as an example the absorption spectrum of **T1-B** is compared with the emission spectrum of the matrix). It also applies to the higher energetic ($\pi-\pi^*$) band of **T3** compounds. However, taking into account significantly lower photoluminescence quantum yields of these luminophores, we decided to test only the **T1** and **T2** compounds as components of the guest/host LEDs.

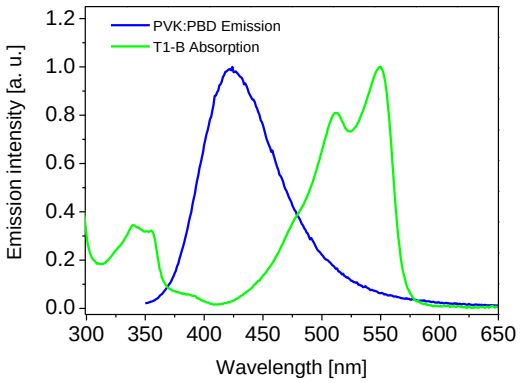

Fig. 13 Emission spectrum of PVK+PBD matrix and absorption spectrum of **T1-B**.

Effective functioning of LEDs in the guest/host configuration must also imply an appropriate alignment of the energy levels between the host matrix components and the guest molecules. Guest luminophore molecules should constitute traps for holes and electrons, in order to increase probability of the exciton formation. This condition is fulfilled when the HOMO level of the guest components is higher than the HOMO levels of the matrix components and the LUMO level of the guest molecules is lower than the LUMO levels of matrix components. This is indeed the case for all studied compounds, as seen in Figure 14.

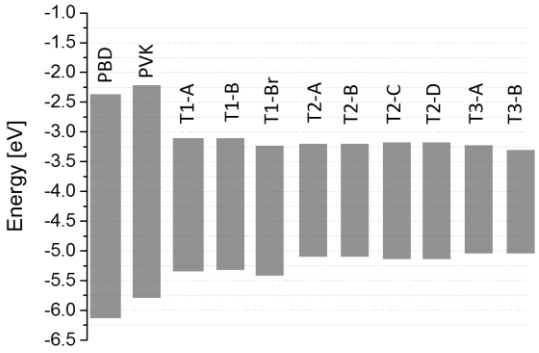

Fig. 14 HOMO and LUMO energy levels for PVK[54,55] and PBD[56] compared with the corresponding levels in diketopyrrolopyrrole derivatives determined electrochemically.

The effective energy transfer from the matrix to the guest is unequivocally confirmed by photo and electroluminescence experiments carried out for layers of PVK+PBD with **T1-B**. Excitation with the wavelength of 345 nm typically used for the excitation of the matrix yields the spectrum typical of the guest with a negligible contribution of spectral features originating from the host even for the concentrations of the guest below 1 wt%. If the excitation wavelength of 535 nm is used, capable of direct exciting the guest but not the host, the spectrum of the guest is also obtained, however four times less intensive.

In Fig. 15 the electroluminescence spectrum of the single layer diode (with active layer consisting of PVK+PBD as a host and **T1-B** as a guest) is compared with the photoluminescence spectrum of the same layer. Apart from minor differences in relative intensities of individual vibronic bands, both spectra are very similar. In the electroluminescence spectrum no contribution from the host can be detected even at as low concentrations of dopant as 0.7 wt%, while in the photoluminescent spectrum some residual emission from the matrix is still visible. This may suggest that the dominant mechanism in OLEDs is related to charge trapping by the dopant rather than Förster energy transfer. Similar behavior has been reported for PVK+PBD matrix with iridium complexes.[52,57,58]

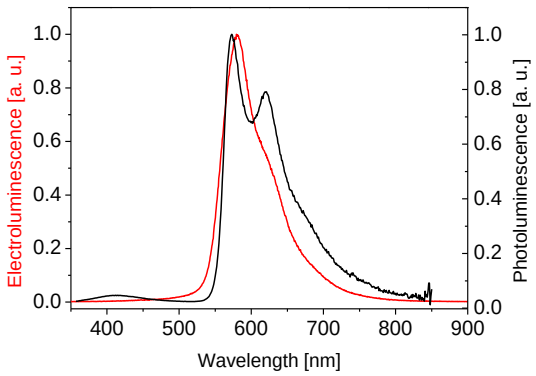

Fig. 15 Photo- and electroluminescence spectra of the guest/host layer consisting of PVK+PBD matrix in which 0.7 wt% of **T1-B** were molecularly dispersed.

Luminophores of **T2** series (**T2-C** and **T2-D**) yield very poorly operating LEDs with a luminance below 50 cd/m^2. Devices with higher luminance can be fabricated from the compounds of **T1** series. Figure 16 presents typical electrical and optical responses of a representative guest/host single layer diode fabricated using **T1-A** as a guest dopant. Diodes fabricated with **T1-B** dopant show very similar behavior. Working parameters of the diodes fabricated from two compounds of **T1** series are collected in Table 5. The measured luminances were in the range between 1300 - 2600 cd/m^2 with luminous efficiency of 0.5-0.7 cd/A. The turn-on voltages for the investigated OLEDs were in the range of 10-13 V. Devices with different dopant concentrations (0.7, 1, 2, 3 wt%) in the active layer were prepared. In the case of **T1** series the best results were obtained for the luminophore content of 1 wt%. Such concentration guarantees an efficient energy transfer and eliminates the fluorescence self-quenching caused by too high concentration.

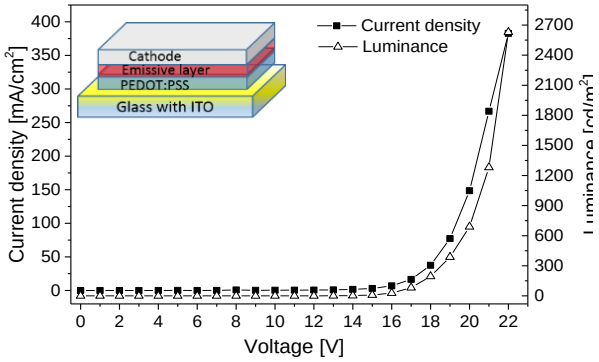

Fig. 16. Typical *I-V-L* characteristics of OLED based on PVK+ PBD with 1 wt% of **T1-A**. Insert: schematic cross-section of fabricated single layer OLED.

Table 5. The best obtained working parameters of OLEDs based on PVK diodes fabricated from compounds of **T1** series (content of the luminophore 1 wt%).

Compound	Luminance (cd/m^2)	Efficiency (cd/A)	El λ_{max}	CIE (x, y)
T1-A	2629	0.7	580	0.52 0.47
T1-B	1870	0.5	581	0.53 0.47

Conclusions

We have carried out detailed studies of redox and spectroscopic properties of DAD semiconductors consisting of diketopyrrolopyrrole central acceptor unit and mono-, bi- or terthiophene donor units. It turned out that their redox properties are weakly dependent on the type of the alkyl N-substituents, however are significantly influenced by the position of the solubilizing alkyl substituent in the donor unit. These findings were perfectly consistent with the results of DFT calculations and in line with the trends found in the absorption spectra of differently substituted compounds. Drastic decrease of the photoluminescence quantum yield was found with increasing length of the D segment, dropping from over 80 % in compounds with monothiophene donor units to 20% in those with terthiophene donor units. The same trend was found in the OLEDs performance with active layer made of PVK+PBD matrix with **T1** and **T2** compounds used as the guest molecules. The devices based on **T2** compounds show rather poor working parameters, while simple, single layer OLEDs with monothiophene diketopyrrolopyrrole derivatives from the **T1** series molecularly dispersed in the PVK+PBD matrix exhibit luminance exceeding 2600 cd/m^2, what indicates that these derivatives are suitable candidates for the fabrication of guest/host type light emitting diodes.

Acknowledgements

This work has been supported in part by the European Union in the framework of Regional Development Fund through the Joint UW and WUT International PhD Program of Foundation for Polish Science – "Towards Advanced Functional Materials and Novel Devices" (MPD/2010/4). G. W-S. acknowledges the financial support of the National Science Centre (Poland) through the Grant No. 2012/04/S/ST4/00128. A.P. acknowledges the financial support of Foundation for the Polish Science Team Programme co-financed by the EU European Regional Development "New solution processable organic and hybrid (organic/inorganic) functional materials for electronics, optoelectronics and spintronics" (Contract No. TEAM/2011-8/6). Quantum-chemical calculations have been supported by the Czech Science Foundation (Project No. 15-05095S).

References

1 C. B. Nielsen, M. Turbiez, I. McCulloch, *Adv. Mater.*, 2013, **25**, 1859.

2 P. Bujak, I. Kulszewicz-Bajer, M. Zagorska, V. Maurel, I. Wielgus, A. Pron, *Chem. Soc. Rev.*, 2013, **42**, 8895.

3 Y. Li, P. Sonar, L. Murphy, W. Hong, *Energy & Environmental Science*, 2013, **6**, 1684.

4 M. J. Robb, S.-Yu. Ku, F. G. Brunetti and C. J. Hawker, *J. of Polymer Sci., Part A: Polym. Chem.*, 2013, **51**, 1263.

5 B. Tieke, A. R. Rabindranath, K. Zhang and Y. Zhu, *Beilstein J. Org. Chem.*, 2010, **6**, 830.

6 S. Qu and H. Tian, *Chem. Commun.*, 2012, **48**, 3039.

7 Y. Zou, D. Gendron, R. Neagu-Plesu, M. Leclerc, *Macromolecules*, 2009, **42**, 6361.

8 A. B. Tamayo, M. Tantiwiwat, B. Walker, T. Q. Nguyen, *J. Phys. Chem. C*, 2008, **112**, 15543.

9 Y. Li, P. Sonar, S. P. Singh, M. S. Soh, M. van Meurs, J. Tan, *J. Am. Chem. Soc.*, 2011, **133**, 2198.

10 S. Stas, S. Sergeyev, Y. Geerts, *Tetrahedron*, 2010, 66, 1837.

11 S.-Y. Liu, M.-M. Shi, J.-C. Huang, Z.-N. Jin, X.-L. Hu, J.-Y. Pan, H.-Y. Li, A. K.-Y. Jen, H.-Z. Chen, *J. Mater. Chem. A.*, 2013, **1**, 2795.

12 M. Gora, W. Krzywiec, J. Mieczkowski, E. C. Rodrigues Maia, G. Louarn, M. Zagorska, A. Pron, *Electrochimica Acta*, 2014, **144**, 211.

13 L. Bürgi, M. Turbiez, R. Pfeiffer, F. Bienewald, H.-J. Kirner, C. Winnewisser, *Adv. Mater.*, 2008, **20**, 2217.

14 Y. Zou, D. Gendron, R. Badrou-Aich, A. Najari, Y. Tao, M. Leclerc, *Macromolecules*, 2009, **42**, 2891.

15 L. Dou, J. Gao, E. Richard, J. You, C. C. Chen, K. C. Cha, Y. He, G. Li, Y. Yang, *J. Am. Chem. Soc.*, 2012, **134**, 10071.

16 A. K. Palai, H. Cho, S. Cho, T. J. Shin, S. Jang, S.-U. Park, S. Pyo, *Org. Electron.*, 2013, **14**, 1396.

17 M. Tantiwiwat, A. Tamayo, N. Luu, X.-D. Dang, T.-Q. Nguyen, *J. Phys. Chem. C* 2008**, 112**, 17402.

18 V. S. Gevaerts, E. M. Herzig, M. Kirkus, K. H. Hendriks, M. M. Wienk, J. Perlich, P. Müller-Buschbaum, R. A. J. Janssen, *Chem. Mater.*, 2014, **26**, 916.

19 C. T. Lee, W. T. Yang, R. G. Parr, *Phys. Rev. B*, 1988, **37**, 785.

20 A. D. Becke, *J. Chem. Phys*., 1993, **98**, 5648.

21 I. S. Ignatyev, T. Sundius, *Chem. Phys. Lett*., 2000, **326**, 101.

22 S. Záliš, I. Kratochvilova, A. Zambova, J. Mbindyo, T. E. Mallouk, T. S. Mayer, *Eur. Phys. J.* E, 2005, **18**, 201.

23 M. Vala, J. Vyňuchal, P. Toman, M. Weiter, S. Luňák Jr., *Dyes and Pigments*, 2010, **84**, 176.

24 M. J. Frisch, G. W. Trucks, H. B. Schlegel, G. E. Scuseria, M. A. Robb, J. R. Cheeseman, G. Scalmani, V. Barone, B. Mennucci, G. A. Petersson, H. Nakatsuji, M. Caricato, X. Li, H. P. Hratchian, A. F. Izmaylov, J. Bloino, G. Zheng, J. L. Sonnenberg, M. Hada, M. Ehara, K. Toyota, R. Fukuda, J. Hasegawa, M. Ishida, T. Nakajima, Y. Honda, O. Kitao, H. Nakai, T. Vreven, J. A. Montgomery, Jr., J. E. Peralta, F. Ogliaro, M. Bearpark, J. J. Heyd, E. Brothers, K. N. Kudin, V. N. Staroverov, T. Keith, R. Kobayashi, J. Normand, K. Raghavachari, A. Rendell, J. C. Burant, S. S. Iyengar, J. Tomasi, M. Cossi, N. Rega, J. M. Millam, M. Klene, J. E. Knox, J. B. Cross, V. Bakken, C. Adamo, J. Jaramillo, R. Gomperts, R. E. Stratmann, O. Yazyev, A. J. Austin, R. Cammi, C. Pomelli, J. W. Ochterski, R. L. Martin, K. Morokuma, V. G. Zakrzewski, G. A. Voth, P. Salvador, J. J. Dannenberg, S. Dapprich, A. D. Daniels, O. Farkas, J. B. Foresman, J. V. Ortiz, J. Cioslowski, D. J. Fox, computer program Gaussian 09, Revision D.01, Gaussian, Inc., Wallingford CT, 2013.

25 J. Tomasi, B. Mennucci, R. Cammi, *Chem. Rev*., 2005, **105**, 2999.

26 R. Bauernschmitt, R. Ahlrichs, *Chem. Phys. Lett*., 1996, **256**, 454.

27 M. E. Casida, C. Jamorski, K. C. Casida, D. R. Salahub, *J. Chem. Phys*., 1998, **108**, 4439.

28 R. E. Stratmann, G. E. Scuseria, M. J. Frisch, *J. Chem. Phys*., 1998, **109**, 8218.

29 J. P. Perdew, K. Burke, and M. Ernzerhof, *Phys. Rev. Lett*., 1996, **77**, 3865.

30 J. P. Perdew, K. Burke, and M. Ernzerhof, *Phys. Rev. Lett*., 1997, **78**, 1396.

31 C. Adamo and V. Barone, *J. Chem. Phys.*, 1999, **110**, 6158.

32 T. Yanai, D. P. Tew, N. C. Handy, *Chem. Phys. Lett.*, 2004, **393**, 51.

33 D. Jacquemin, E. A. Perpète, G. E. Scuseria, I. Ciofini, C. Adamo, *J. Chem. Theory Comput.*, 2008, **4**, 123.

34 V. Barone, J. Bloino, M. Biczysko: Vibrationally-resolved electronic spectra in GAUSSIAN 09, white paper of GAUSSIAN 09 Revision A.02, September 2, 2009.

35 F. Santoro, R. Improta, A. Lami, J. Bloino, and V. Barone, *J. Chem. Phys*., 2007, **126**, 084509.

36 V. Barone, J. Bloino, M. Biczysko, and F. Santoro, *J. Chem. Theory and Comput.*, 2009, **5**, 540.

37 R. Improta, V. Barone, G. Scalmani, and M. J. Frisch, *J. Chem. Phys*., 2006, **125**, 054103.

38 R. Improta, G. Scalmani, M. J. Frisch, and V. Barone, J. Chem. Phys., 2007, **127**, 0745504.

39 H. Bürckstümmer , A. Weissenstein , D. Bialas, F. Würthner, *J. Org. Chem.*, 2011, **76**, 2426.

40 A. K. Palai, J. Lee, M. Jea, H. Na, T. J. Shin, S. Jang, S.-U. Park, S. Pyo, *J. Mater. Sci.*, 2014, **49**, 4215.

41 M. A. Naik, N. Venkatramaiah, C. Kanimozhi, S. Patil, *J. Phys. Chem. C*, 2012. **116**, 26128.

42 H. Liu, H. Jia, L. Wang, Y. Wu, C. Zhan, H. Fu, J. Yao, *Phys. Chem. Chem. Phys.*, 2012, **14**, 14262.

43 B. Zhao, K. Sun, F. Xue, J. Ouyang, *Org. Electron.*, 2012, **13**, 2516.

44 M. Kirkus, L. Wang, S. Mothy, D. Beljonne, J. Cornil, R. A. J. Janssen, S. C. J. Meskers, *J. Phys. Chem. A*, 2012, **116**, 7927.

45 R. A. J. Janssen, L. Smilowitz, N. S. Sariciftci, D. Moses, *J. Chem. Phys.*, 1994, **101**, 1787.

46 B. Wardle, *Principles and Applications of Photochemistry*, John Wiley & Sons, 2009, 66.

47 M. Kasha, *Radiat. Res.* 1963, **20**, 55–70**,**

48 A. S. Davidov, *Theory of Molecular Excitons*; Plenum Press: NewYork, 1971.

49 M. A. Baldo, S. Lamansky, P. E. Burrows, M. E. Thompson, S. R. Forrest, *Appl. Phys. Lett.*, 1999, **75**, 4.

50 D.-Y. Lee, M.-H. Lee, Ch.-J. Lee, S.-K. Park, *Electron. Mater. Lett.*, 2013, **9**, 663.

51 X. Yang, D. Neher, D. Hertel, T.K. Daubler, *Adv. Mater.*, 2004, **16**, 161.

52 B. Luszczynska, E. Dobruchowska, I. Glowacki, J. Ulanski, F. Jaiser, X. Yang, D. Neher and A. Danel, *J. Appl. Phys.*, 2006, **99**, 24505.

53 H. Meng, N. Herron, in *Organic Light-Emitting Materials and Devices*, edited by Z. Li and H. Meng (Boca Raton, 2007), 295-412.

54 J. An, J. Chang, J. Han, C. Im, Y.-J. Yu, D.H. Choi, J.-I Jin, T. Majima, *J. Photochem. & Photobiol. A: Chem.*, 2008, **200**, 371.

55 F.-C. Chen, S. C. Chang, G. He, S. Pyo, Y. Yang, M. Kurotaki, J. Kido, *J. Polym. Sci., Part B: Polym. Phys.*, 2003, **41**, 2681.

56 S.-C. Chang, G. He, F.-C. Chen, T.-F. Guo, Y. Yang, *Appl. Phys. Lett.,* 2001, **79**, 2088.

57 X. Gong, J. C. Ostrowski, D. Moses, G. C. Bazan, A. J. Heeger, *Adv. Funct. Mater.*, 2003, **13**, 439 and references therein.

58 I. Glowacki and Z. Szamel, *J. Phys. D: Appl. Phys.*, 2010, **43**, 295101.